The Quantum Well Self-Electrooptic Effect Device: Optoelectronic Bistability and Oscillation, and Self-Linearized Modulation

DAVID A. B. MILLER, MEMBER, IEEE, DANIEL S. CHEMLA, THEODORE C. DAMEN, THOMAS H. WOOD, MEMBER, IEEE, CHARLES A. BURRUS, JR., FELLOW, IEEE, ARTHUR C. GOSSARD, AND WILLIAM WIEGMANN

Abstract—**We report extended experimental and theoretical results for the quantum well self-electrooptic effect devices. Four modes of operation are demonstrated: 1) optical bistability, 2) electrical bistability, 3) simultaneous optical and electronic self-oscillation, and 4) self-linearized modulation and optical level shifting. All of these can be observed at room-temperature with a CW laser diode as the light source. Bistability can be observed with 18 nW of incident power, or with 30 ns switching time at 1.6 mW with a reciprocal relation between switching power and speed. We also now report bistability with low electrical bias voltages (e.g., 2 V) using a constant current load. Negative resistance self-oscillation is observed with an inductive load; this imposes a self-modulation on the transmitted optical beam. With current bias, self-linearized modulation is obtained, with absorbed optical power linearly proportional to current. This is extended to demonstrate light-by-light modulation and incoherent-to-incoherent conversion using a separate photodiode. The nature of the optoelectronic feedback underlying the operation of the devices is discussed, and the physical mechanisms which give rise to the very low optical switching energy (~4 fJ/μm^2) are discussed.**

I. Introduction

MULTIPLE quantum well structures (MQWS) consisting of alternate thin layers of GaAs and AlGaAs have recently become interesting for their optical properties. One exceptional property of the MQWS is the existence of clearly-resolved exciton absorption peaks near the optical absorption edge at room temperature [1]–[4]. Most normal semiconductors show well-resolved peaks only at low temperature; with increasing temperature the collisions with the increasing density of optical photons result in severe broadening. However, the quantum confinement of the electrons and holes in the GaAs layers within a thickness (e.g., 100 Å) much less than the normal exciton diameter in GaAs (about 300 Å) makes the exciton binding energy (the separation of the resonances from the bandgap) larger without further increasing the phonon broadening; this and other consequences of the quantum confinement can explain the persistence of the resonances to room temperature [2], [5], [6]. (One incidental consequence of the confinement is that it also removes the degeneracy in the valence bands of the semiconductor resulting in two exciton resonances, the "light hole" and heavy hole" excitons.) The existence of these resonances has led among other things to the study of their nonlinear optical properties [1], [2], [5], [6], such as absorption saturation and the associated nonlinear refraction.

However, the present paper is concerned with another consequence of the excitons which appears to be even more dependent on the quantum confinement of the carriers. When an electric field is applied perpendicular to the quantum well layers, the whole absorption edge (including the exciton resonances) moves to lower photon energies [7]–[9]. This is remarkable because normal semiconductors do not show this effect at any temperature. The consequence of applying electric fields to conventional semiconductors is the Franz–Keldysh effect [10], which is primarily a broadening of the bandedge with comparatively little shift; the exciton peaks broaden and disappear at low fields. However for the perpendicular fields in the MQWS, the excitons remain resolved to high fields. This effect in the MWQS has recently been explained through a novel mechanism called the quantum-confined Stark effect (QCSE) [8], [9].

The cause of the broadening of the exciton resonances with increasing field is basically the reduction of exciton life time due to field ionization; the electron and hole are ripped apart by the applied field. In the MQWS, there are two consequences of confinement which inhibit this ionization: 1) the potential barriers presented by the walls of the wells (i.e., the larger bandgap AlGaAs layers) inhibit the electron and hole from tunneling completely away from one another; 2) even if the electron and hole are pulled almost completely to opposite sides of the GaAs wells, the wells are so thin that there is still strong Coulomb interaction and strong bound electron-hole states (excitons) still exist. As a consequence, very large fields can be applied without broadening the exciton. The formalism for solving the problem of the shift of the exciton resonances reduces to that of the Stark shift of a confined hydrogen atom [8], [9], hence the title QCSE. Shifts of 2.5 times the zero-field binding energy are possible at 50 times the classical ionization field.

Manuscript received January 24, 1985.

D. A. B. Miller, D. S. Chemla, and T. C. Damen are with AT&T Bell Laboratories, Holmdel, NJ 07733.
T. H. Wood and C. A. Burrus, Jr., are with AT&T Bell Laboratories, Crawford Hill, NJ 07733.
A. C. Gossard and W. Wiegmann are with AT&T Bell Laboratories, Murray Hill, NJ 07947.

0018-9197/85/0900-1462$01.00 © 1985 IEEE

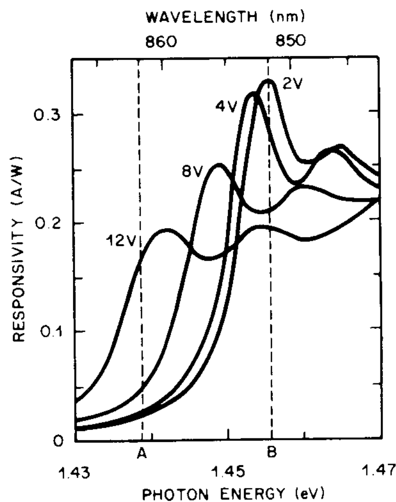

Fig. 1. Responsivity as a function of wavelength for various reverse bias voltages as shown for the p-i-n structure. Point A is 861.8 nm; point B is 851.7 nm; 600 μm diameter sample.

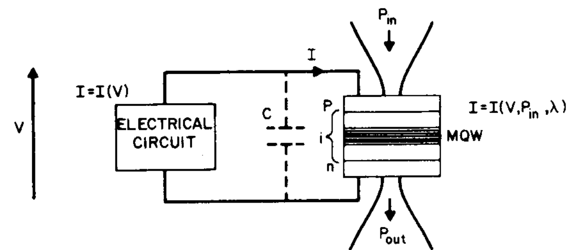

Fig. 2. Generalized schematic diagram for the SEED configuration. When it is necessary to consider the time dependence of the circuit, we will separate the capacitance of the p-i-n diode as if it were an external component, as shown by the dashed capacitor C.

Because the QCSE gives a shift of a large absorption, modulators can be made with only microns of material [7], [11]. These devices are also capable of high-speed operation, so far tested down to 131 ps [11]. The same structures used to demonstrate modulation can also, however, function as optical detectors. In fact, we find that we can obtain approximately unit internal quantum efficiency in the p-i-n structure with the quantum wells in the i region as discussed in detail below, i.e., one carrier (pair) is collected for every photon absorbed [9]. One incidental consequence of this is that the QCSE can equally well be monitored through the photocurrent spectra; a set of spectra are shown in Fig. 1 for several different voltages across the structure. The shift of the exciton peaks can be clearly resolved. The peak at lower photon energy is the heavy hole exciton peak, and the smaller peak at higher photon energy is the light hole exciton peak. This simultaneous operation as a modulator and photo detector is also the basis of the self electrooptic device (SEED), which we discuss in this paper.

The general principle of the SEED is that the photocurrent passing through an electronic circuit influences the voltage across the modulator; the voltage across the modulator influences the absorption of light by the modulator and hence, influences the photocurrent. Thus a feedback is established. This feedback is truly optoelectronic: without the light shining on the device, there is no photocurrent and no change in photocurrent with voltage due to the change in optical absorption; in turn, the electrical circuit determines the way in which the change in photocurrent changes the voltage. The general schematic of the SEED is shown in Fig. 2. While the SEED configurations discussed here are certainly hybrid in that they involve both optics and electronics, the SEED is intrinsically an integrated form of device, and furthermore these configurations do not require any active electronic components or external gain for their operation.

The behavior of the SEED depends greatly on the nature of the electronic circuit and on the sign of the feedback. Under positive feedback we obtain bistability or oscillation. The bistability has previously been reported by us briefly [12]. The oscillation is a new mode of operation which, from constant electrical and optical bias, gives both electrical and optical oscillation. Under negative feedback, totally different behavior is obtained; so far, self-linearized modulation, linear light-by-light modulation, and optical level shifting have been demonstrated [13].

The SEED's are interesting for a number of reasons. First, they represent a novel class of optoelectronic devices without a close precedent [14]–[17]; it is therefore interesting to understand how they operate and the physical principles underlying their behavior, and that understanding is the main purpose of this paper. Second, they represent a new opportunity for devices, and they may offer novel solutions to existing or future problems. Third, they operate under very practical conditions: they run at room-temperature; they operate at wavelength and powers compatible with light-emitting or laser diodes and at voltages compatible with semiconductor electronics; they are compatible in materials and growth technology with both electronics and semiconductor light sources, suggesting the possibility of integration, and they offer very low energy operation.

The layout of this paper is as follows. In Section II the experimental samples, apparatus, and methods will be briefly discussed. In Section III we will present the general theoretical framework for the SEED modeling. The nature of the optical bistability will be investigated in Section IV, and the associated electrical bistability will be discussed in Section V. In Section VI, the oscillator will be described. The operation as a self-linearized modulator and optical level shifter will be examined in Section VII. The scaling arguments on operating energies will be presented in Section VIII, and the overall conclusions of the work will be given in Section IX.

II. Experimental Details

To apply an electric field perpendicular to the MQWS layers we grew a p-i-n diode structure with the quantum wells in the intrinsic region of the diode. There are two reasons for choosing this structure to implement the SEED's. First, reverse biasing the diode can give large fields across the wells without large currents flowing,

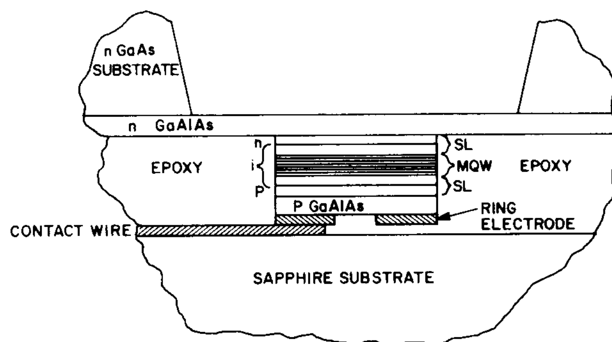

Fig. 3. Schematic diagram of the 100 μm mesa sample (not to scale) showing the layer structure of the material. The n-contact is taken off the substrate. The p-contact is through the gold ring electrode and the contact wire as shown. The total epitaxial layer thickness is 3.9 μm and the thicknesses of these layers are shown greatly exaggerated for clarity. The aluminum mole fraction is 0.32 in all GaAlAs layers. p- and n-doping levels were both 5×10^{17} cm^{-3}. The doped GaAlAs layers are both 0.98 μm thick. The multiple quantum well (MQW) region is 0.97 μm thick, and consists of 50 periods of 95 Å GaAs and 98 Å GaAlAs. The superlattice (SL) consists of 28.5 Å GaAs layers alternating with 68.5 Å GaAlAs layers. Doped superlattice regions are 0.19 μm (20 periods) thick. Undoped (i) superlattice regions are 0.29 μm (30 periods) thick. The mesa diameter is 100 μm, and the hole in the ring electrode is 25 μm diameter. The sample is epoxied to the sapphire substrate after the mesa etch.

which allows efficient operation and eliminates possible thermal problems. Second, this structure is ideally suited for simultaneous operation as a detector. We have found empirically [9] that the responsivity of this structure corresponds to unit internal quantum efficiency, within experimental error, for all reverse bias voltages greater than 2 V. This agrees well with our estimate that above about 2 V the depletion region extends throughout the MQWS region [7], [9].

We will not discuss the material structure and growth in great detail here as it is more extensively discussed elsewhere [7], [9]. The detailed layer thicknesses and compositions are given in the caption to Fig. 3. The material used in these SEED experiments is grown by molecular beam epitaxy and is the same as that used by us for modulator experiments [7] and investigations of the QCSE [8], [9]. The layer sequence is as shown in the sample schematic diagram of Fig. 3. Starting with a silicon—(i.e., n-doped) GaAs substrate, a transparent n-doped GaAlAs layer is grown. Above this a transparent superlattice buffer region is grown, first n-doped and then undoped to form the start of the intrinsic region of the diode. Next, the 50 95 Å GaAs quantum well layers alternate with 98 Å GaAlAs barriers to form the MQWS. Then, the sequence of undoped superlattice, doped superlattice and doped GaAlAs is grown, this time with p-doping. The thinness of the GaAs layers in the superlattice (28.5 Å) ensures that the optical absorption of this material is quantum-shifted to wavelengths shorter than those of interest here.

To make the samples for the experiments, we have formed a mesa in the epitaxial layers as shown in Fig. 3 to define a small area diode. The electrical contact on the p-doped top contact is formed by zinc diffusion, gold alloying, and plating to leave a gold-plated ring electrode with a hole in the center. To allow optical access, the GaAs substrate is etched away beneath the mesa using a selective etch. Two samples are used in the present study. One has a 600 μm diameter mesa with a 100 μm diameter hole in the electrode; this sample is used for all experiments unless otherwise stated. The second sample (shown schematically in Fig. 3) has a 100 μm diameter mesa with a 25 μm diameter electrode hole; this sample is epoxied to a sapphire substrate as shown.

An LDS 821 continuous-wave dye laser pumped by a krypton-ion laser was used for all experiments unless otherwise stated. We also used a Hitachi HLP 1400 diode laser for all the experiments with the 100 μm sample. The diode laser was temperature-tuned over a range of 5 nm. For bistability experiments with the dye laser, the power was modulated using an acoustooptic modulator. With the diode laser, the power was modulated by varying the current of the diode. In both cases, neutral density filters were used as necessary to reduce the overall power in the optical beam. Detection was with silicon photodiodes, with an avalanche diode used for high-speed measurements. Powers were measured with a UDT 161 power meter.

III. Formal Description of SEED Behavior

In general, the feedback behavior of the SEED devices can be described in terms of two simultaneous relations. One relation describes the detection properties of the quantum well structure (as shown in Fig. 1), giving the current I through the modulator as a function of the voltage V on the modulator, the optical input power P_{in}, and the wavelength λ of the incident light,

$$I = I(V, P_{in}, \lambda). \quad (1)$$

The other relation describes the behavior of the circuit to which the modulator is connected, i.e., the relation between I and V imposed by the circuit

$$I = I(V). \quad (2)$$

In this description, (2) is the "load line" of the circuit, and the current I will depend on other circuit parameters not explicitly stated here, such as supply voltage or component values. Solving these two equations simultaneously to eliminate I will give the relation between P_{in} and V at a given wavelength, and the internal behavior of the device will be understood in terms of both optical and electrical parameters.

One further simple relation is required to deduce the output power from the input power, namely the modulator transmission function for the output optical power P_{out},

$$P_{out} = P_{out}(P_{in}, V, \lambda). \quad (3)$$

For all the situations in this paper the detector equation (1) reduces to the simple relation

$$I = S(V, \lambda)\, P_{in} \quad (4)$$

where S is the measured responsivity of the detector (in A/W) as a function of voltage and wavelength. We can

make this simplification because the leakage current of the diode is negligible, and the responsivity of the diode (at fixed wavelength and voltage) empirically does not depend on power over the range of powers we use. For (3), the transmission function also simplifies to give

$$P_{\text{out}} = T(V, \lambda)\, P_{\text{in}} \tag{5}$$

where T is the measured transmission as a function of voltage and wavelength, because the transmission also empirically does not depend on power in our conditions. In fact, because the internal quantum efficiency is constant (approximately unity) for all reverse bias voltages above 2 V, the absorption closely follows the absorbed power and the transmission looks like a mirror image of the responsivity (see Fig. 4).

The behavior of all of the SEED configurations so far demonstrated can be described by these relations. The feedback in the system is contained in the interplay between relations (1) [or (4)] and (2). When $I(V)$ in (2) is not explicitly time-dependent (e.g., it contains no capacitors, or inductors, or time varying drive voltages or currents) we can formally deduce whether the feedback is positive or negative at a given (equilibrium) solution of (4) and (2) by performing a linearized stability analysis. This is a valid approach for the bistability and self-linearized modulation (we will consider the oscillator separately below in Section VI). Consider for example the change in voltage v about the equilibrium point. We presume there is a finite capacitance C associated with the device for mathematical convenience as shown dashed in Fig. 2; this is also physically realistic as the device does have capacitance due to the depletion region. We obtain, by expanding to first order about the equilibrium solutions,

$$C \frac{dv}{dt} = \left[\frac{dI}{dV} - P_{\text{in}} \frac{dS}{dV} \right] v. \tag{6}$$

If the term in square brackets is positive, v will diverge exponentially, the solution is unstable, and the feedback is positive. Conversely, if this term is negative, so also is the feedback, v settles exponentially and the solution is stable.

In all the configurations considered here, the electrical circuit to which the quantum wells are connected will have positive slope resistance corresponding to negative dI/dV with the current convention shown in Fig. 2. The sign of the feedback can only be positive if $P_{\text{in}}\, dS/dV$ is negative, and then only if

$$P_{\text{in}} \frac{dS}{dV} < \frac{dI}{dV} \tag{7}$$

which becomes the condition for instability. In other words, as long as S increases with V, the solutions are stable, but if S decreases with V, the solutions can be unstable depending on the rest of the cirucit.

Illustrative operating wavelengths (photon energies) for the two feedback modes are shown on Fig. 1. At a photon energy below the zero-field heavy-hole exciton peak position such as at point A in Fig. 1, increasing voltage V will give increasing responsivity S over the entire voltage range shown, so all solutions at this wavelength are stable over this range. However at point B in Fig. 1, as the exciton peaks move past the operating wavelength, the responsivity S can decrease with increasing voltage V and instability is possible.

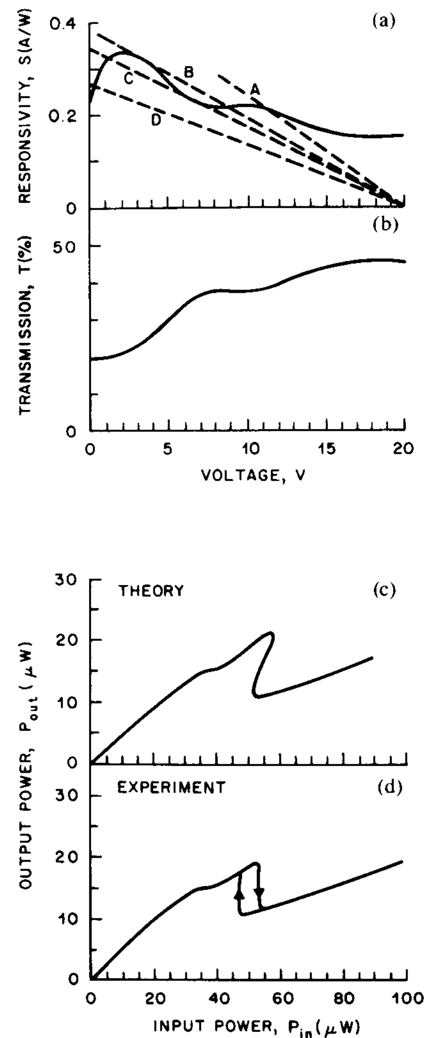

Fig. 4. Graphical solution method for bistable SEED behavior with a simple resistive load. (a) The solid line is the measured responsivity at 851.7 nm with reverse bias, V [see (1)]. This is the same wavelength as point B on Fig. 1. The dashed lines A–D are the load lines imposed by the circuit (equation (2)) for various increasing values of the input optical power, P_{in}. The intercept of these lines with the horizontal axis is the supply voltage, V_0, which is 20 V in this example. Lines A and D show only one intersection (i.e., only one solution); all lines between B and C show three intersection points, corresponding to bistability. As discussed in the text, the middle of these three points is unstable. (b) The measured optical transmission of the p-i-n diode, also at 851.7 nm. (c) The theoretical optical input/output characteristic calculated using the measured responsivity and transmission with R = 1 MΩ and V_0 = 20 V as described in the text; there are no fitted parameters. (d) The measured optical input/output characteristic at 851.7 nm with R = 1 MΩ and V = 20 V. All measurements are for the 600 μm diameter sample.

Another way of viewing the positive feedback in the device is to note its close connection with negative differential conductance. At constant power the differential conductance of the p-i-n diode is $P_{\text{in}}\, dS/dV$, so that the diode shows negative differential conductance whenever S decreases with V. This is true over several ranges of voltages

and wavelengths as can be seen in Fig 4(a). The operation of electrical bistability (Section V) and the oscillator (Section VI) can both be understood as consequences of this negative conductance in a manner analogous to purely electrical negative conductance circuits such as those utilizing tunnel diodes [18]. It must be remembered, however, that this negative conductance results from an optoelectronic feedback. Unlike the tunnel diode, the whole scale of the electrical characteristic (including the negative conductance) can be altered by changing the optical input power, and the optical bistability is not, therefore, analogous to any simple electrical circuit; it is, however, true that the optical bistability cannot exist without the existence of negative differential conductance at some power and voltage.

That optical and electrical bistability should be so interrelated is a consequence of a more general principle. Bistability is basically a simple cusp catastrophe [19]. One consequence of this is that, if the system is bistable with respect to variation of one parameter, we can expect that it will be bistable with respect to others. Thus, for example in Fabry–Perot bistability, the system is bistable under variation of the input power, and also under variation of wavelength and cavity tuning or some combination of all three. In the present case, since supply voltage is a parameter of the system, we should expect to see bistability with respect to supply voltage when the optical input conditions are held fixed. This will be discussed in Section V. In another case where the circuit parameters are altered with a second light beam, we also see bistability with respect to the variation of power in the second light beam. This is discussed in Section IV-B.

IV. SEED Optical Bistability

A. Resistive Load

The simple circuit that we use for optical bistability with a resistive load is shown schematically in Fig. 5. A constant reverse bias voltage V_0 is connected through a series resistor to the p-i-n diode. The current equation (2) becomes

$$I = (V_0 - V)/R \tag{8}$$

where R is the value of the series resistance. Using (4) we may rewrite this as

$$S = \frac{(V_0 - V)}{RP_{\text{in}}}. \tag{9}$$

For various P_{in}, this gives us the straight lines in Fig. 4(a). The detector equation (1) at constant wavelength can be formally rewritten using (4) as

$$S = S(V) \tag{10}$$

(i.e., the measured responsivity function for a given wavelength). A specific measured function appears as the curve in Fig. 4(a). The particular curve shown is the measured responsivity at the wavelength of the heavy hole exciton peak at zero field. At first, the responsivity rises with in-

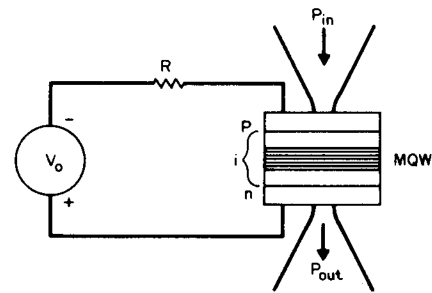

Fig. 5. Schematic diagram for optical bistability with a simple resistive load.

creasing voltage because the quantum efficiency is rising as the depletion region extends throughout the device. Then the responsivity falls because the exciton peak moves to lower photon energies. The subsequent peak near 10 V is due to the light hole exciton peak moving through the operating wavelength. This behavior is consistent with the transmission curve of Fig. 4(b).

The simultaneous solution of (1) and (2) then reduces to the graphical solution on Fig. 4(a); the solutions are the intersections of line and curve. The lines with triple intersections (between lines B and C) correspond to the powers for which bistability is possible. Applying the stability criterion equation (7) it can be seen that the middle intersection is an unstable solution and the others are stable. The criterion for the existence of bistability can be deduced directly from this graphical method, from the criterion in [20] (the relation to [20] is discussed below) or from the instability criterion equation (7) (above) since the bistability cannot exist without one unstable point. Hence, using (7) and (4)

$$\frac{dS}{dV} < \frac{S}{V - V_0}. \tag{11}$$

For bistability to exist at a given V_0 and λ, this criterion must be satisfied for some range of V.

A nongraphical modeling method is the simple "backwards" technique of choosing a voltage V, deducing S from the measured responsivity (8), and hence deducing P_{in} from (7). By either method, the relation between P_{in} and V is obtained. Finally, the relation between P_{out} and P_{in} as shown in Fig. 4(c) is obtained for the particular wavelength from the measured transmission function (5) [Fig. 4(b)]. The curve shows the classic "S" shape for optical bistability.

In Fig. 4(d), we show an experimental result taken using the same parameters as used in the theoretical curve [Fig. 4(c)]. There are no adjustable parameters in the theory, and the agreement with experiment is good. Clear bistability is seen, with switching transitions at the edges of the hysteresis region.

As has been pointed out [12], [20], this bistability is an example of optical bistability from increasing absorption. This class of bistability requires no mirrors, cavities, or other external optical feedback. Various examples of this bistability class have been independently demonstrated or proposed; many of these have recently been summarized

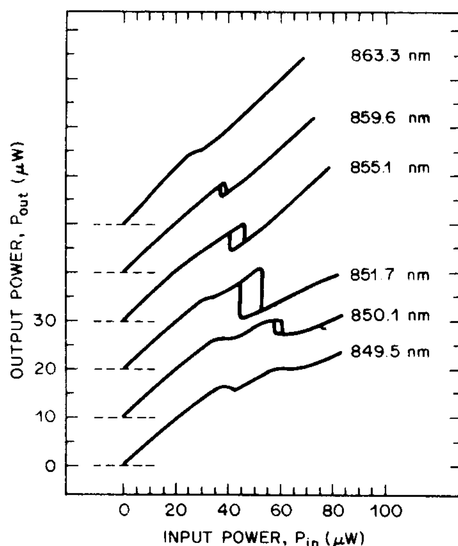

Fig. 6. Input/output characteristic as a function of operating wavelength with the circuit as shown in Fig. 5. The zeros are displaced on successive spectra for clarity as shown by the dashed lines. V_0 = 20 V; R = 1 MΩ, 600 μm diameter sample.

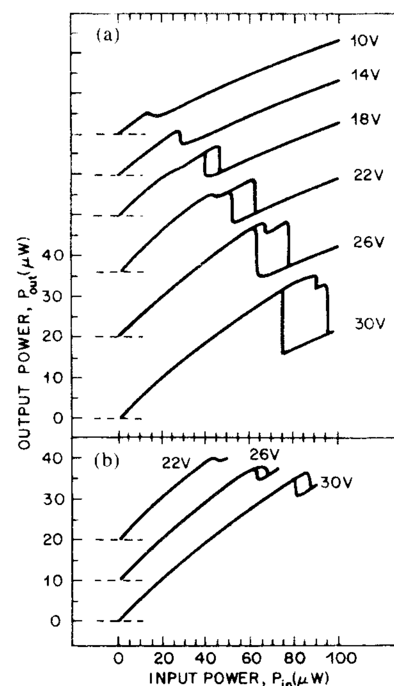

Fig. 7. Input/output characteristics as a function of supply voltage V_0 with the circuit as shown in Fig. 5. The zeros are displaced on successive spectra for clarity as shown by the dashed lines. (a) Curves without restrictions on input power, showing overlapping bistable regions above 26 V; (b) Curves with maximum input power restricted to show light hole bistability while avoiding second (heavy-hole) bistable transition. λ = 851.7 nm; R = 1 MΩ; 600 μm diameter sample.

[20]. The general feedback mechanism of this class relies on having a material (or system) in which the fraction of the incident light absorbed (the absorption) increases as the material becomes more excited. Then as the incident power increases the material becomes more excited, thus further increasing the absorption, which in turn makes the material even more excited, and so on. Thus a positive feedback is established which can lead to switching under the right conditions.

The relations (9) and (10) are of exactly the same functional form as the general relations (2) and (1) of [20] if we choose for the measure of the degree of excitation of the system the voltage change $V_0 - V$, and if instead of the actual fractional absorption A we use the responsivity S. This latter slight formal departure is of little importance; the responsivity is proportional to the absorption over most of the voltage region of interest.

The behavior of the input/output characteristic as a function of operating wavelength is shown in Fig. 6. Bistability is seen over a comparatively large range of wavelengths (861.8–850.1 nm at 20 V bias). The width of the bistable region also exemplifies one of the predictions of the theory of this class of bistability [20], that the width of the bistable region is largely determined by the ratio between the absorption in the high and low transmission states; larger contrast between the two states should give larger width.

The behavior of the optical input/output characteristic as a funciton of bias voltage V_0 is shown in Fig. 7. Bistability is seen for all voltages above 14 V for this wavelength (851.7 nm). With increasing voltage, the "kink" in the characteristic seen just below the bistable region at, for example, 22 V on Fig. 7(a) develops into a bistable region itself. This second bistability results from the light-hole exciton peak; as can be visualized from Fig. 4(a), if the voltage is increased enough eventually multiple intersections of straight lines and curve will be possible through the light-hole peak. This bistability can overlap the other bistable region. At 26 and 30 V, two "switch-down" transitions are seen although only one "switch-up" is apparent; this is a consequence of the precise functional shape of the responsivity curve. The light-hole bistability can be viewed separately by restricting the maximum input power so that the heavy-hole bistability threshold is not reached as shown in Fig. 7(b).

The curves in Figs. 4, 6, and 7 are deliberately taken at slow scan rates of the incident power. With increasing scan rates, the switching transitions are no longer sharp due to the finite switching times. The switching times depend very much on how rapidly the input power is ramped, with rapid ramping of the input giving sharper switching transitions. The hysteretic regions also broaden as the input power is ramped more rapidly due to delays in the switching. Both of these phenomena are characteristic of the effect known as "critical slowing down" [21] seen in bistable switching systems. (One simple mathematical manifestation of critical slowing down can be seen in the linearized limit in (6); at the critical points for switching the term in square brackets vanishes; thus although the point is not truly stable, the system will take an infinite time to switch.) There is thus no simple definition for the switching time of the system.

The switching down (i.e., from high to low transmission) is also generally less affected by the critical slowing-down and all the times we discuss will be for this transition. The switch up is typically about a factor of two

TABLE I

Resistance (R)	Switching Power	Switching Time	RC Time Constant	Switching Energy Per Unit Area (fJ/μm^2)
600 μm sample				
100 MΩ	670 nW	1.5 ms	2 ms	3.5
10 MΩ	6.5 μW	180 μs	200 μs	4.2
1 MΩ	66 μW	20 μs	20 μs	4.6
100 kΩ	660 μW	2.5 μs	2 μs	6.0
22 kΩ	3.7 mW	400 ns	440 ns	5.3
100 μm sample				
1.1 GΩ	107 nW	1 ms	660 μs	14
22 MΩ	4.9 μW	20 μs	13 μs	12
47 kΩ	1.6 mW	30 ns	28 ns	6.1

slower. We find empirically that there is a limit to how much the switching can be speeded up by overdriving the input, thus enabling us to define a limiting switching time. With slowly varying input powers, the switching time typically lengthened by a factor of 4-5. For example, the 30 ns switching time measured for the 100 μm diameter sample listed in Table I was taken with the input power ramped up and down in 600 ns. Ramping up and down in 8 μs gave a switching time of 140 ns. This behavior is characteristic of critical slowing down, with the switching time tending to limit towards the underlying time constant of the system as the switching is strongly over-driven [21].

Table I lists (limiting) switching times for both of the samples with a variety of different resistors. These times were measured with 20 V bias at 853 nm. All of the measurements on the 100 μm sample were taken using the diode laser as the light source. To emphasize the scaling, we have listed the switching energy per unit area, this being the product of the limiting switching time and the switching power divided by the area of the mesa. We have also tabulated the RC time constants in each case. We use a measured capacitance of 20 pF for the 600 μm sample and an estimated capacitance of 600 fF for the 100 μm sample (stray capacitances in the circuit make any more accurate measurement of the capacitance difficult for this sample). The overall accuracy in switching time measurements is only about a factor of two due to laser noise.

For both samples, the switching time clearly scales with the RC time constant of the system, and the switching power scales inversely with the resistance, as would be expected theoretically. The switching energy per unit area remains remarkably constant over the wide range of switching times reported; the variation in switching energy per unit area is within experimental error when stray capacitance is taken into account for the smaller sample. Slower switching was not possible for the 600 μm sample because the leakage current of the diode then became dominant. The proportionality between switching time and total RC time constant was, however, retained when external capacitors were added in parallel with the sample to slow down the switching.

With the 100 μm sample we were able to obtain optical bistability with 18 nW of incident power by using three reverse-biased silicon diodes in series instead of the load resistor. The leakage current of the diodes in series was about 3 nA with 20 V bias, giving an effective resistance of about 6 GΩ. The switching time was 40 ms; this is somewhat longer than expected from scaling, but we attribute this to the capacitance of the diodes.

B. Constant Current Load

As can be seen from Fig. 7, with increasing bias voltage V_0 the bistability becomes easier to achieve and the loop becomes broader. The bistability occurs at higher input powers, but if we also proportionately increased the load resistance R as we increased V_0, the switching power would remain approximately constant. This behavior is easily understood from the graphical solution of Fig. 4. With V_0 and R increasing in proportion, the intercept of the straight load lines with the horizontal axis moves further to the right and the load lines become more horizontal while still retaining exactly the same intercept with the vertical axis. The more horizontal the load lines become, the easier it is to satisfy the condition for bistability, (7), because dI/dV becomes less negative. This suggests that, for the best bistability, we should use very large voltages and resistance. In the limit of infinite voltage and resistance, $dI/dV = 0$, bistability is possible in principle with even the slightest negative slope dS/dV. High voltages are not, however, desirable for various reasons. One disadvantage of high voltages is high electrical switching energy because of the requirement to charge the capacitance of the p-i-n diode to a large fraction of this voltage for switching.

An alternative method which embodies many of the advantages of the above method without some of the disadvantages is to use a constant current bias circuit. An idealized circuit is shown in Fig. 8(a) and two of the many possible practical circuits for synthesizing a constant current source are shown in Fig 8(b) and (c). For the moment we will only consider the circuit in Fig. 8(b); we will return to use both circuits in the discussion of negative feedback operation with current bias (Section VII). Here we have used a tungsten bulb to illuminate the silicon photodiode in Fig. 8(b) with incoherent light. With this control light shining on the photodiode, this diode passes an ap-

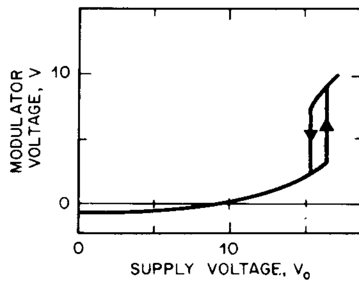

Fig. 8. Constant current circuits. (a) Idealized schematic for the SEED under current bias. (b) Constant current source with current value controlled by the amount of light shining on the silicon photodiode. (c) Constant current source with current value controlled by the control voltage V_c.

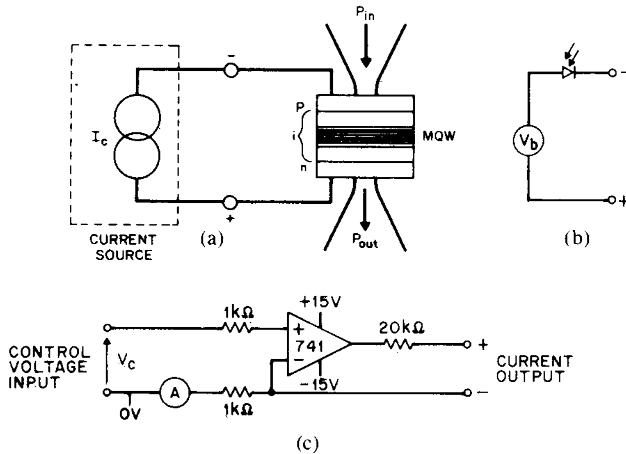

Fig. 9. Optical input/output characteristics at 853 nm for the 100 μm sample using the constant current circuit of Fig. 8(b) with reverse bias supply voltages V_b between 0 and 6 V as shown, 9.3 μA constant current bias. The zeros are displaced on successive spectra for clarity as shown by the dahed lines.

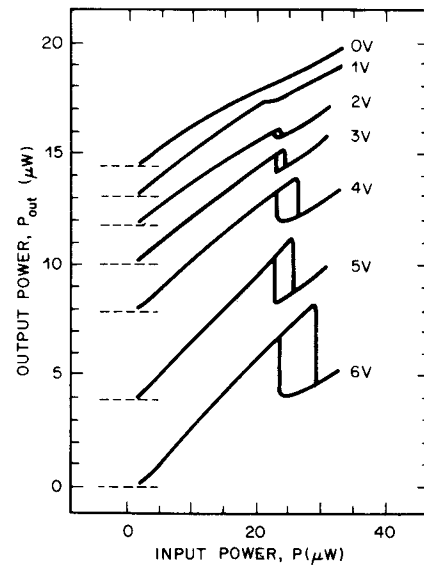

Fig. 10. Voltage V across the p-i-n modulator as supply voltage V_0 is varied. The electrical circuit is as shown in Fig. 5. Optical input power and wavelength are held constant at 46 μW and 852.4 nm respectively. R = 1 MΩ; measuring probe impedance (in parallel with p-i-n) 10 MΩ; 600 μm diameter sample.

proximately constant current as long as it is reverse biased between 1 and 6 V. Within these limits therefore, dI/dV is approximately zero, and bistability should be easily achieved. (We restricted the supply voltage to 6 V or less in our experiments.) This constant current is the photocurrent, and its value can be controlled by adjusting the intensity of the tungsten bulb light shining on it. This circuit, in common with the many other methods of generating constant currents, can only operate up to a finite voltage output; when the output voltage from the circuit approaches the supply voltage, the current starts to drop off. (In the present case the photocurrent decreases as the voltage across the diode drops below 1 V.) For our present purposes, we can treat the load line of the constant current source as being horizontal for output voltages up to about 1 V less than the supply voltage, and as falling off nearly vertically towards the horizontal axis thereafter. Thus, even for low supply voltages, we can achieve the three intersections of load line and curve necessary for bistability.

Typical results are shown in Fig. 9 for bistability with the photodiode load using the laser diode as the light source for the 100 μm diameter p-i-n modulator with 6 V supply voltage. Note the total absence of any kink in the curve from the light hole resonance; this is because the voltage is never high enough to move the light hole resonance to the operating wavelength. With this circuit, we were able to observe bistability with as little as 2 V supply voltage. By contrast, with the resistive load discussed above, 14 V were necessary. This type of constant current loading therefore can greatly reduce the operating voltage for bistability, which is ultimately important for limiting electrical energies in switching applications. The present circuit does not show particularly fast switching compared to that seen at similar switching powers with the resistive load, presumably because of the depletion capacitance of the photodiode.

One incidental feature of this particular configuration is that the switching power can be controlled optically by adjusting the amount of control light (in this case from the tungsten bulb) landing on the silicon photodiode. The bistability can also be set and reset by slight variations of this control power, and the system is also therefore bistable with respect to variation of the control power at constant laser power. Note that the control power can be from a broad-band incoherent light source as in this case, or from any other convenient source.

V. Electrical Bistability

As discussed in Section III, we should expect bistability with respect to variation of supply voltage because of the existence of negative differential conductance and for fundamental reasons. In Fig. 10 we show electrical bistability observed with this system. We use the circuit of Fig. 5 except that now we vary the supply voltage V_0 and hold the optical input power constant. This bistability can be observed either in the voltage across the device (as in Fig. 10) or in the optical transmission as the supply voltage is varied. (The optical bistability as a function of input power

can, of course, be monitored equally well through the voltage across the device.)

The behavior of the electrical bistability can be understood through a graphical analysis similar to that of Fig. 4; now instead of varying the slope of the straight lines as a constant intercept (the fixed V_0), the slope of the lines is held fixed and the intercept is varied (the varying V_0). As can be seen in Fig. 10, the voltage V starts out below the axis; this corresponds to the p-i-n being in forward bias from its own photocurrent. (The responsivity S falls off in forward bias (not shown on Fig. 4) to reach zero near the built-in voltage of the diode.) With increasing V_0, the system eventually switches to the high-voltage, low-optical absorption state.

The existence of electrical bistability also implies that optical bistability can be set and reset electrically. We have tested this directly. With the various parameters set so that the system is in the middle of a bistability loop, a momentary decrease of V_0 switched the system from the high (optical) transmission state to the low transmission state, and a momentary increase would switch it back. Voltage changes of ~ 1 V were usually sufficient to achieve this, corresponding to the width of the electrical bistable region as in Fig. 10.

VI. Negative Resistance Optoelectronic Oscillation

As discussed in Section III, because of the existence of negative differential conductivity, we should expect to be able to demonstrate a negative resistance (or conductance) oscillator by an analogy with similar circuits using tunnel diodes. A simple formal schematic for such a circuit is shown in Fig. 11. For formal convenience we have shown the capacitance C of the p-i-n diode as if it were separate from the diode. This fiction enables us to retain relation (4) to describe the diode, even in this time-dependent case, as there are no other time-dependent terms expected in the diode behavior on the timescales of interest here. It also means that we can treat any additional capacitance added in parallel with the diode with the same theory. Using (4) and analyzing the circuit of Fig. 11, we obtain

$$\frac{d^2V}{dt^2} + \left(\frac{R_l}{L} + \frac{P_{\text{in}}}{C}\frac{dS}{dV}\right)\frac{dV}{dt} + \frac{1}{LC} \cdot (V - R_l P_{\text{in}} S(V) - V_b) = 0 \tag{12}$$

at constant optical power and wavelength. We will not attempt to solve this large signal relation. However, for small signals (12) reduces to

$$\frac{d^2v}{dt^2} + \left(\frac{R_l}{L} + \frac{P_{\text{in}}}{C}\frac{dS}{dV}\right)\frac{dv}{dt} + \frac{1}{LC}\left(1 + P_{\text{in}} R_l \frac{dS}{dV}\right) v = 0 \tag{13}$$

where we have expanded S to first order about V_b and v is the departure of the voltage V from equilibrium. For this standard equation for a damped oscillator the condition for self-oscillation is

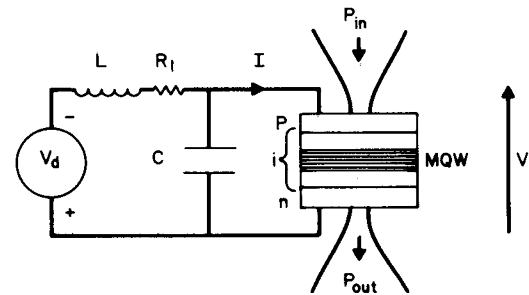

Fig. 11. Idealized circuit for optoelectronic oscillator, with C as the capacitance of the diode (and other parallel capacitance), L as the inductance, R_l as the series loss resistance of the circuit, and V_d as the supply voltage. V is the voltage across the diode.

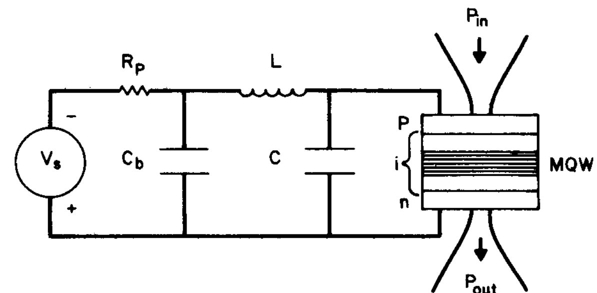

Fig. 12. Actual circuit for oscillator. The series loss resistance is not explicitly shown. The supply voltage V_s is somewhat larger than the idealized mean reverse bias voltage V_d of Fig. 11 because of the voltage drop across series protection resistor R_p from the mean dc bias current of the device.

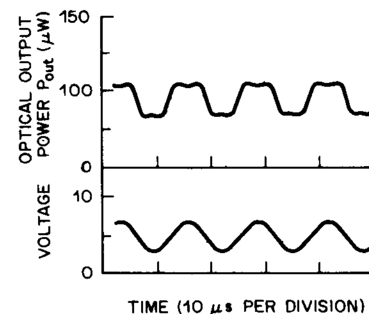

Fig. 13. Simultaneous optical and electronic self-oscillation of the SEED circuit of Fig. 12. The voltage is the voltage V as shown in Fig. 12 as measured using a ×100 10 MΩ 2.2 pF probe. The 100 μm diameter sample is used with 430 μW incident power P_{in} from the laser diode at 852 nm. Inductance L: 97 mH. Bypass capacitor C_b: 100 nF. Oscillator capacitance C: stray capacitance of inductor in parallel with other stray capacitance and probe and modulator capacitances. 100 μm diameter sample. Supply voltage V_s: 7 V. Mean dc reverse bias voltage V_d (i.e., dc voltage measured across bypass capacitor C_b): 4.9 V.

$$P_{\text{in}} \frac{dS}{dV} < -R_l \frac{C}{L}. \tag{14}$$

We were able to observe oscillation with the practical circuit shown in Fig. 12. The supply voltage now has a series protection resistor and an additional large bypass capacitor has been added as an ac short to give the dc power supply negligible ac impedance despite the presence of the series resistor; for ac purposes the two circuits are essentially identical. A typical pair of traces of the optical and electronic oscillations is shown in Fig. 13, in this case taken with the 100 μm sample and the CW laser diode.

We performed an extended series of experiments with the 600 μm sample and the dye laser source. It was not possible to resolve the power for the onset of true oscillation because of laser noise; fluctuations in the laser power can cause the circuit to "ring" even if it is below the true threshold for self-oscillation. At 851.7 nm, oscillation was clear above 40 μW between 5.3 and 5.9 V supply voltage V_s; this observation is consistent with the form of the responsivity curve in Fig. 4(a), which shows its largest negative slope, and hence its largest negative conductance, near 5-6 V. With increasing power the range of the supply voltage over which oscillation was observed increased; this is also consistent with the form of the responsivity since, with increasing power, the whole scale of the negative conductances is correspondingly increased, hence permitting oscillation over a larger voltage range. With 300 μW we were able to observe oscillation between 11.3 and 25.2 V supply voltage. (At this power the voltage drop across the series protection resistor is not negligible, and we estimate it at 4-8 V. The actual bias voltage at the p-i-n is correspondingly smaller.)

In all cases in which the oscillation was clear it was a large signal oscillation; as can be seen on Fig. 13, the optical modulation is consequently deep and not sinusoidal, although the electrical oscillation is more nearly sinusoidal. With the 600 μm sample, the electrical oscillation was generally so large that it extended into forward bias (the trace goes below the axis).

With incident powers of 150 to 300 μW and optimization of the supply voltage, oscillation could be observed with input wavelengths from 840.4 to 861.1 nm. At higher voltages and powers (e.g., at 150 μW between 14.5 and 17.0 V) it was also possible to resolve a second region of oscillation of smaller amplitude which we ascribe to the negative resistance associated with the light hole exciton.

Using a variety of inductors from 97 down to 0.12 mH we observed oscillation from 53 kHz to 1.88 MHz using the 600 μm sample without any added capacitance. These frequencies were somewhat lower than the oscillation frequency expected using 20 pF for the internal capacitance of the diode; the effective capacitance required to explain the observed frequency varied from inductor to inductor, and the explanation may be stray capacitance in the inductors themselves. With large amounts of added capacitance, the frequency approaches the expected value. We expect that higher frequecies would be attainable with improved inductors and packaging.

VII. Self-Linearized Modulation and Optical Level Shifting

One simple characteristic of any equilibrium state (stable or unstable) of the general SEED circuit in Fig. 2 is that the photocurrent as given by (1) or (4) equals the current through the electrical circuit, as can be deduced directly from conservation of current. As mentioned above, the p-i-n diode used shows, empirically, unit internal quantum efficiency above about 2 V reverse bias. In this range, therefore, the absorption A can be written

$$A = \frac{\hbar\omega}{e} S. \tag{14}$$

The optical power absorbed in the device is $P_a = P_{in}A$, and the (photo)current is $I = SP_{in}$. Hence, using (14),

$$P_a = \frac{\hbar\omega}{e} I. \tag{15}$$

Consequently, in any equilibrium state the absorbed power is proportional to the current flowing round the circuit, regardless of the nature of the circuit.

As was discussed in Section III, if the device is operated under conditions in which dS/dV is positive and dI/dV for the circuit is negative (corresponding to positive resistance in the circuit), the optoelectronic feedback is negative and the equilibrium state is stable. Consequently, the system will stay in the equilibrium state and the absorbed power will be proportional to the circuit current. If we can control the current linearly with some external parameter, we can utilize this property to make linear optical modulators, with absorbed power proportional to that parameter.

To make the current dependent only on some external control parameter requires that it be independent of the internal voltage V; we must therefore design "constant current" circuits in which the current is independent of voltage and whose current setting I_c [see Fig. 8(a)] is controlled by an appropriate external parameter. There are many ways of achieving this; two such circuits are shown in Fig. 8. Fig. 8(b) shows a constant current circuit controlled by light and Fig. 8(c) shows one controlled by voltage V_c.

With a constant current source, it is particularly easy to understand the operation of the circuit directly. In the generalized circuit shown in Fig. 8(a), the action of the current from the constant current source is to charge up the capacitance of the diode, whereas the action of the photocurrent generated in the diode is to discharge it. If the photocurrent is less than the source current I_c, the voltage across the diode starts to rise. However, because dS/dV is positive, the photocurrent rises. Conversely, if the photocurrent exceeds I_c, the voltage starts to fall, which in turn makes the photocurrent decrease. Thus, the point with equal photocurrent and source current is stable, and because the absorbed power and photocurrent are proportional, the absorbed power is set proportional to the source current. This proportionality exists because of the feedback and not because of any intrinsic linearity in the modulation; the modulation with voltage is far from linear. Because the linearity results from feedback, we call this mode of operation self-linearized modulation.

Fig. 14 shows the transmitted optical power as a function of current for various input powers. Beyond a "knee" in the characteristic the output power decreases linearly with increasing current with coefficient $\hbar\omega/e$ as expected from (15). This set of data was actually taken using the voltage-controlled constant current circuit shown in Fig. 8(c), and the form of the curves is identical within exper-

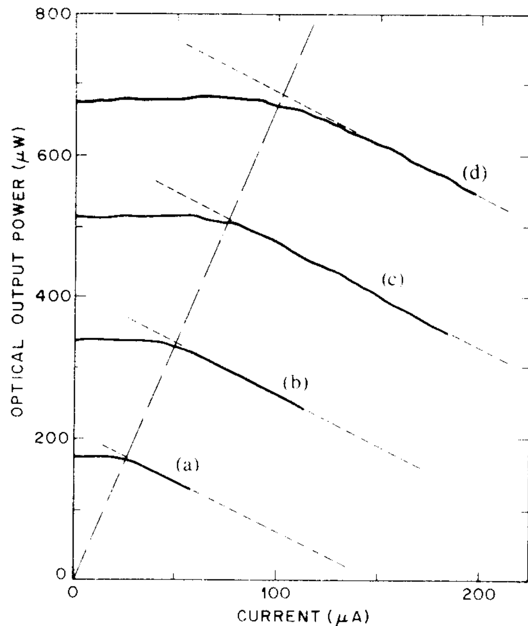

Fig. 14. Optical output power as a function of the current at a wavelength of 855.8 nm for four different optical input powers with the 600 μm diameter sample. (a) 330 μW, (b) 650 μW, (c) 980 μW, and (d) 1.3 mW. The dashed lines have slope $-\hbar\omega/e$ as expected from (15) for unit internal quantum efficiency. The dotted-dashed line has a slope of 150 mA/W, corresponding to the responsivity of the device near 2 V reverse bias at 855.8 nm.

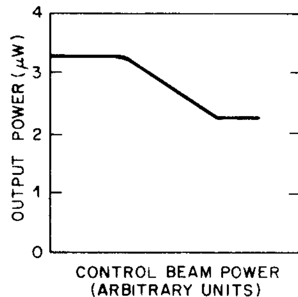

Fig. 15. Control of the transmitted laser power (vertical axis) by the incoherent light power (horizontal axis) incident on a silicon photodiode using the circuit of Fig. 8(b). Incident diode laser power: 9.4 μW. Laser wavelength: 855 nm. 100 μm diameter sample. Reverse bias supply voltage, V_b: 6 V.

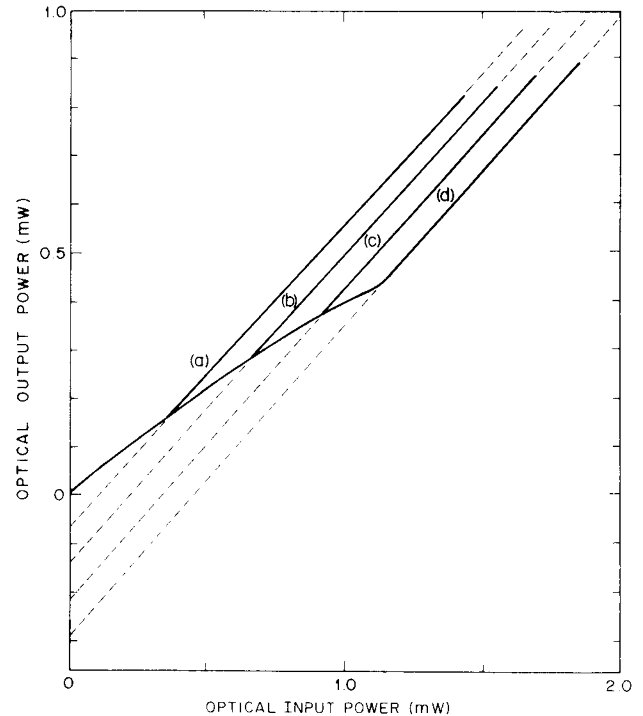

Fig. 16. Optical level shifter action (subtraction of constant optical base lines) for the SEED under constant current bias with the circuit of Fig. 8(c). Bias currents: (a) 50 μA, (b) 100 μA, (c) 150 μA and (d) 200 μA. Dye laser wavelength 858.0 nm. The dashed lines are parallel, with intercepts on the output power axis of $-\hbar\omega I_c/e$, where I_c is the appropriate constant bias current, as predicted by (15).

imental error if the transmitted power is plotted against control voltage. The reason for the "knee" and the constant transmitted power below this point on each curve is that the modulator at any given operating wavelength has a minimum absorption; once this minimum is reached the transmitted power cannot be increased further. Below the "knee," the voltage across the modulator reduces and eventually goes into forward bias. This reduction results in the breakdown of the proportionality between absorbed power and photocurrent [see (15)] because the quantum efficiency drops off. The "knee" actually corresponds to the point at which this proportionality starts to break down (i.e., below about 2 V reverse bias), and the slope of the dashed line that indicates the "knee" in Fig. 14 is, correspondingly, approximately the reciprocal of the responsivity at 2 V reverse bias.

Fig. 15 shows a result similar to those of Fig. 14, this time taken with the light-controlled constant current source of Fig. 8(b). In this case, the silicon photodiode produces a photocurrent, almost independent of reverse bias supply voltage V_b between 1 and 6 V, that is linearly proportional to the amount of light shining on it. The horizontal axis in Fig. 15 is the light power from a tungsten filament bulb as measured with a separate detector. Light from the same bulb is focused onto the silicon photodiode and the brightness of the bulb is altered to give the characteristic as shown in Fig. 15. The vertical axis is the laser beam power transmitted through the modulator. This system also behaves as a self-linearized modulator, this time controlled by an incoherent light source. Increasing tungsten bulb power gives decreasing transmitted laser power; hence this system behaves as a linearized, inverting, light-by-light modulator and incoherent-to-coherent converter. With increasing tungsten bulb power, this characteristic shows a second "knee" after the self-linearized region in which the transmitted laser power is again independent of the incident tungsten bulb power. In this region, increasing bulb power gives no further increase in bias current as the voltage across the silicon photodiode is low (e.g., less than 1 V reverse bias) and its responsivity decreases.

The final mode of operation of the SEED device that will be considered here is the optical level shifter configuration. This is the same as the self-linearized modulator except that the bias current is held constant and the optical input power is varied. A typical set of optical input/output characteristics taken with several different bias currents is shown in Fig. 16. To the right of the "knees" in these

characteristics, the operation is exactly the same as in the self-linearized modulator, in that the optical power absorbed is proportional only to the bias current; this proportionality remains when the optical power is varied and the bias current is held constant (the opposite situation to that described for the self-linearized modulator above) as can be deduced from (15). Thus, for constant bias current [derived in this case from the circuit of Fig. 8(c)] a constant optical power is absorbed. When the characteristics above the "knee" are projected back to the vertical axis, they intercept at the (negative) powers predicted by (15) for unit internal quantum efficiency. The "knee" in the characteristics occurs in this case because there is a limit to the maximum absorption of which the modulator is capable at a given wavelength; below the "knee" either the constant current source can give no further increase in voltage or (as in this case) the modulator can give no further increase in absorption regardless of any further increase in voltage. The effect of this configuration is to subtract a constant optical "base line" from the transmitted power above the "knee," hence the title of optical level shifter. Better contrast between the two regions of the characteristic would be possible for devices with higher peak absorption (e.g., thicker modulators).

The behavior of the optical level shifter is related to the bistability under current bias discussed above in Section IV-B. In fact, the region to the left of the bistable loops in the characteristics shown in Fig. 9 actually starts out as an optical level shifter characteristic at powers too low to be clearly resolved on Fig. 9. The optical level shifter behavior breaks down at powers somewhat higher than those in Fig. 15 because there is a maximum transmission of the modulator at any given wavelength, and all the curves in Fig. 15 eventually limit to the maximum transmission line. This causes the negative feedback to break down; positive feedback then becomes possible, and bistability can take place.

VIII. Performance Scaling

One of the features that makes the SEED devices of practical interest is their low operating energy. Operating energies are important for two reasons: 1) some power source is required to run the devices (e.g., a laser), and low operating energies help reduce these power requirements; 2) thermal conduction of the dissipated energy sets a limit to how often, and how many, devices can be operated. High operating energies have long been a problem for optical switching devices. In this section, we will briefly discuss the physics behind the operating energy and the scaling of the energy with various parameters. We also consider the scaling of the switching time.

There are several ways of looking at operating energy of an optical switch. First, we could consider the incident energy in a light beam required to make enough change in the optical properties of the material to swing the output of the system from one logic level to the other; this is essentially the energy considered by Smith [22] in his scaling arguments on optical switching energies. The absorbed or dissipated optical energy may be less than this estimate. The extent to which critical slowing down increases these energies depends on how the system is driven, and we will not consider this in any detail. Second, we should also consider energy requirements and dissipation from any other energy source; in the present case, we must consider the electrical energy and dissipation.

In the case of the SEED, we can estimate, from first principles and from the known properties of the QCSE, the requirements on absorbed optical energy, stored electrostatic energy, and dissipated electrical energy during a switching transition.

To make the devices operate in any logic mode, we must substantially change the optical properties of the material. All the present device configurations rely on the change of the optical absorption. These configurations also rely on only a single pass of the light beam through the material. While multiple passes and/or resonant cavities are possible, we will not consider these here. Hence we must make the material sufficiently thick so that the change in absorption is strong as the device goes from one state to the other (e.g., one absorption length). Because the absorption changes from the QCSE can be of the order of 5000–10 000 cm^{-1}, we therefore require at least 1 μm material thickness. To make these changes in absorption, we require fields of $\sim$ 50 kV/cm in the quantum well material. Thus electrostatic energy must be stored in the material to operate the device. An equivalent way to view this energy is as the energy required to charge up the capacitance of the device. To charge a capacitor C to a steady-state voltage V, in addition to storing $(\frac{1}{2})\,CV^2$ energy in the capacitor, dissipates at least as much energy in the (resistive) circuit used to charge it up, regardless of the resistance of the circuit. (With an inductor, it is possible to charge up the capacitor without dissipating this energy, but the voltage oscillates and the state is not steady.) Hence for any logical operation, at least this amount of stored electrostatic energy must be dissipated. While we could use more material and charge it with a lower field, this would be less efficient in stored electrostatic energy because the change in absorption with much lower fields is more than proportionately lower. Since the capacitance of a 1 μm sheet of this material is $\sim$ 100 aF for every square square micron of area, we expect a minimum dissipated energy of $\sim$ 1.3 fJ/μm^2 to operate the device, and the total dissipated electrical energy should scale linearly with the area of the device because the capacitance does.

In the device configurations considered here, the only means of discharging the capacitance of the device is the photocurrent; the current from the power supply always charges the capacitance of the device (to increasing reverse bias). Hence we can deduce a minimum optical energy to operate the device. The charge density required to discharge the capacitance is $Q = CV$, which for the numbers used here is 500 aC/μm^2. One photon must be absorbed for every electronic charge on (either) plate. The photon energy is about 1.5 eV; consequently about 750

aJ/μm^2 optical energy must be absorbed in every switching cycle. The incident optical energy must be somewhat larger (e.g., by a factor of 2) as a useful amount of light must be transmitted. Hence we might expect an incident optical energy limit of about 1.5 fJ/μm^2. Note that this energy density refers to the area of the device, not the area of the optical beam. Again we expect this energy to scale with device area.

These physical arguments therefore predict limiting total operating energies of ~ 3 fJ/μm^2. Scaling to a hypothetical limiting device of area $(\lambda)^2/n^2$ (where n is the refractive index) to compare with the limits of [22] gives an incident optical switching energy of 120 aJ (about 500 photons). This very low energy is achieved despite the absence of a resonant cavity to reduce switching energy; other scalings in [22] assume a resonator finesse of 30 with a proportionate reduction in scaled switching energy. We will now compare the behavior of the actual devices with these limits. First, as can be seen from Table I, the switching energy is independent of the switching time over a large range. This is expected from the switching energy argument above and also from the general theory of the bistable switching. Switching power should be inversely proportional to the resistance R, switching time should be proportional to the RC time constant, and hence their product should be constant. Second, the optical and electrical switching energies in Table I compare well with the energy densities predicted above when the increased operating voltage of the bistability with a resistive load is taken into account. Instead of a field of 50 kV/cm, the modulator is run at up to 125 kV/cm. Consequently, 2.5 times as much optical energy should be required because 2.5 times as much charge must be created to neutralize this field. Hence we should expect incident optical energies of about 4 fJ/μm^2, in agreement with the measurements. The electrical energies are larger because of the increased field (by a factor of $(2.5)^2$) and also because of the superlattice buffer regions which increase the field volume by a factor of 1.6. Hence we should expect electrical energies of about 13 fJ/μm^2. Again this is in reasonable agreement with the results in Table I. Furthermore, we have demonstrated that switching can be obtained with lower bias voltages (e.g., 6 V) with the constant current load, so that high voltages are not a fundamental requirement for switching.

These switching energies per unit area compare very favorably with other demonstrated optically bistable switches at comparable wavelengths. In contrast to other optically bistable switches, because of the nature of our device we find no variation in switching power with optical spot size up to the maximum optically allowed, and consequently we compare the size of our device with the optical spot size in other systems in evaluating switching energy per unit area. GaAs–AlGaAs etalon devices [23] may show switching energies of the order of hundreds of fJ/μm^2. Only the very high finesse (~ 420) Na atomic beam system [24] shows energies per unit area comparable to those of the SEED, to our knowledge.

The lower limit on switching time with the SEED devices is not currently clear. The results with the two different samples do show the scaling expected with decreasing capacitance. We have tested the operation of the device as a modulator down to 131 ps, and tests of the samples as detectors showed circuit limited response times of <2 ns. However, 20 ns was the fastest switching time we could observe with the 100 μm sample. With more power the switching transition disappeared. One possible cause of the disappearance is local heating of the sample, which may move the operating point of the device and defeat the bistability. Smaller samples and better heat sinking may improve this performance.

IX. Conclusions

Using the SEED concept of internal optoelectronic feedback combined with the novel quantum-confined Stark effect modulator, we have been able to demonstrate a variety of devices under practical operating conditions, and have been able to understand their operation from simple arguments.

The SEED's have a number of attractive practical features. Their operating power can be scaled over a large range with reciprocal variation in switching time. They run at room temperature. No optical resonators are used, simplifying fabrication and tuning of the devices. The devices are insensitive to the form or area of the light beam as long as it all lands on the device. Although we have not discussed it here, it should also be possible to operate these devices with multiple input beams for logic functions. It is not necessary that the beams spatially overlap on the device; they can be incident on different areas, which incidentally can prevent problems due to interference of mutually coherent beams. Furthermore, because no optical resonators are required, it is not even necessary that the beams be coherent; we have been able to operate all of the configurations here with the dye laser running broad-band (e.g., 3 nm bandwidth) or the diode laser running below threshold. Operation is, however, certainly better if the incident light is narrow-band (e.g., the bistable loops narrow with increasing spectral bandwidth).

All of the configurations presented here can be operated with a commercial cw diode laser. The devices interface readily with semiconductor electronics, and they are truly optoelectronic in that they can operate with optical and/or electronic control inputs and optical and/or electronic signal outputs. The GaAs-based material system is compatible with both electronics and diode lasers, suggesting the possibility of integration.

Finally, the switching energy of the devices is extremely low; this arises from the magnitude of the recently-discovered QCSE and the high quantum efficiency of the internal optical detection. While there are many features to be considered in interpreting switching energies, the basic operating energy of the SEED is arguably so low that high operating energy is no longer a fundamental argument against optical switching.

ACKNOWLEDGMENT

We acknowledge the expert assistance of J. E. Henry in sample preparation.

REFERENCES

[1] D. A. B. Miller, D. S. Chemla, P. W. Smith, A. C. Gossard, and W. T. Tsang, "Room-temperature saturation characteristics of GaAs/GaAlAs multiple quantum well structures and of the bulk GaAs," *Appl. Phys.*, vol. B28, pp. 96-97, 1982.

[2] D. A. B. Miller, D. S. Chemla, D. J. Eilenberger, P. W. Smith, A. C. Gossard, and W. T. Tsang, "Large room-temperature optical nonlinearity in GaAs/$Ga_{1-x}Al_xAs$ multiple quantum well structures," *Appl. Phys. Lett.*, vol. 41, pp. 679-681, 1982.

[3] T. Ishibashi, S. Tarucha, and H. Okamoto, "Exciton associated optical absorption spectra of AlAs/GaAs superlattices at 300 K," in *Proc. Int. Symp. GaAs Related Compounds, Inst. Phys. Conf.*, Japan, 1981, pp. 587-588.

[4] S. W. Kirchoefer, N. Holonyak, K. Hess, D. A. Gulino, H. G. Drickamer, J. J. Coleman and P. D. Dapkus, "Absorption measurements at high pressure on AlAs-$Al_xGa_{1-x}As$-GaAs superlattices," *Appl. Phys. Lett.*, vol. 40, pp. 821-824, 1982.

[5] D. S. Chemla, D. A. B. Miller, P. W. Smith, A. C. Gossard, and W. Wiegmann, "Room temperature excitonic nonlinear absorption and refraction in GaAs/AlGaAs multiple quantum well structures," *IEEE J. Quantum Electron.*, vol. QE-20, pp. 265-275, 1984.

[6] D. S. Chemla and D. A. B. Miller, "Room-temperature excitonic nonlinear-optical effects in semiconductor quantum well structures," *J. Opt. Soc. Amer.*, vol. B2, pp. 1155-1173, 1985.

[7] T. H. Wood, C. A. Burrus, D. A. B. Miller, D. S. Chemla, T. C. Damen, A. C. Gossard, and W. Wiegmann, "High-speed optical modulation with GaAs/GaAlAs quantum wells in a p-i-n diode structure," *Appl. Phys. Lett.*, vol. 44, pp. 16-18, 1984.

[8] D. A. B. Miller, D. S. Chemla, T. C. Damen, A. C. Gossard, W. Wiegmann, T. H. Wood, and C. A. Burrus, "Bandedge electroabsorption in quantum well structures: The quantum confined Stark effect," *Phys. Rev. Lett.*, vol. 53, pp. 2173-2177, 1984.

[9] —, "Electric field dependence of optical absorption near the bandgap of quantum well structures," *Phys. Rev.*, vol. B32, p. 1043, 1985.

[10] For a discussion of the Franz-Keldysh effect and the broadening of exciton resonances with field see J. D. Dow and D. Redfield, "Electroabsorption in semiconductors: The excitonic absorption edge," *Phys. Rev.*, vol. B1, pp. 3358-3371, 1970.

[11] T. H. Wood, C. A. Burrus, D. A. B. Miller, D. S. Chemla, T. C. Damen, A. C. Gossard, and W. Wiegmann, "131 ps optical modulation in semiconductor multiple quantum wells," *IEEE J. Quantum Electron.*, vol. QE-21, pp. 117-118, 1985.

[12] D. A. B. Miller, D. S. Chemla, T. C. Damen, A. C. Gossard, W. Wiegmann, T. H. Wood, and C. A. Burrus, "Novel hybrid optically bistable switch: The quantum well self electro-optic effect device," *Appl. Phys. Lett.*, vol. 45, pp. 13-15, 1984.

[13] D. A. B. Miller, D. S. Chemla, T. C. Damen, T. H. Wood, C. A. Burrus, A. C. Gossard, and W. Wiegmann, "Optical level shifter and self-linearized optical modulator using a quantum-well self-electro-optic effect device," *Optics Lett.*, vol. 9, pp. 567-569, 1984.

[14] Perhaps the closest precedent to the SEED devices is in the interesting work that has been performed on devices using the Franz-Keldysh effect in diodes [15]-[17]. One configuration utilizes the diode in a resonator; this has been considered both theoretically [15] and experimentally [16]. As in the SEED devices reported here, the modulator and photodiode are the same p-n junction. The Franz-Keldysh effect can however only usefully give an increase in absorption with increasing voltage; consequently, the mechanism of bistability from increasing absorption (with decreasing voltage) used in the SEED device (see Section III) is not available and instead a resonator is used as in conventional absorptive bistability to achieve bistability with decreasing absorption. The Franz-Keldysh bistability is therefore a hybrid implementation of conventional absorption bistability. Another configuration using the Franz-Keldysh effect, with an additional separate photodiode for detection and an external transistor to give the gain for bistability, has also recently been reported [17]. Because of the transistor, the cavity is not necessary, and, as in the SEED devices reported here, coherent light is no longer required.

[15] B. S. Ryvkin, "Falling current-voltage characteristic and optical bistability of a resonator photocell in the Franz-Keldysh effect," *Sov. Phys. Semicond.*, vol. 15, pp. 796-798, 1981 (translation of *Fiz. Tekh. Poluprovodn.*, vol. 15, pp. 1380-1384, 1981.

[16] B. S. Ryvkin and M. N. Stepanova, "Bistable optical characteristics of a resonator photocell with two-step optical transitions," *Sov. Tech. Phys. Lett.*, vol. 8, pp. 413-414, 1982 (translation of *Pis'ma Zh. Tekh. Fiz.*, vol. 8, pp. 951-954, 1982).

[17] M. I. Nemenov, B. S. Ryvkin, and M. N. Stepanova, "Optical bistability due to the Franz-Keldysh effect with incoherent unpolarized light," *Sov. Tech. Phys. Lett.*, vol. 9, pp. 260-262, 1983 (translation of *Pis'ma Zh. Tekh. Fiz.*, vol. 9, pp. 604-609, 1983.

[18] M. A. Lee, B. Easter, and H. A. Bell, *Tunnel Diodes*. London, England: Chapman and Hall, 1967.

[19] G. P. Agrawal and H. J. Carmichael, "Optical bistability through nonlinear dispersion and absorption," *Phys. Rev.*, vol. A19, pp. 2074-2086, 1979.

[20] D. A. B. Miller, "Optical bistability and differential gain resulting from absorption increasing with excitation," *J. Opt. Soc. Amer.*, vol. B1, pp. 857-864, 1984.

[21] E. Garmire, J. H. Marburger, S. D. Allen, and H. G. Winful, "Transient response of hybrid bistable optical devices," *Appl. Phys. Lett.*, vol. 34, pp. 374-376, 1979.

[22] P. W. Smith, "On the physical limits of digital optical switching and logic elements," *Bell Syst. Tech. J.*, vol. 61, pp. 1975-1993, 1982.

[23] S. S. Tarng, H. M. Gibbs, J. L. Jewell, N. Peyghambarian, A. C. Gossard, T. Venkatesan, and W. Wiegmann, "Use of a diode laser to observe room-temperature, low-power optical bistability in a GaAs-AlGaAs etalon," *Appl. Phys. Lett.*, vol. 44, pp. 360-361, 1984.

[24] D. E. Grant and H. J. Kimble, "Transient response in absorption bistability," *Optics Commun.*, vol. 44, pp. 415-420, 1983

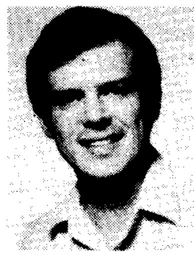

David A. B. Miller (M'84) was born in Hamilton, U.K., in 1954. He received the B.Sc. degree in physics from the University of St. Andrews, St. Andrews, Scotland, in 1976 and the Ph.D. degree from Heriot-Watt University, Edinburgh, Scotland, in 1979.

He remained at Heriot-Watt University until 1981, latterly as a Lecturer in the Department of Physics, before moving to Bell Laboratories, Holmdel, NJ, where he is currently a member of the Technical Staff in the Department of Laser Science Research. His research interests include low-power nonlinear optical effects in semiconductors and optical bistability.

Daniel S. Chemla was born in Tunis, Tunisia, on July 21, 1940. He graduated from L'Ecole Nationale Superieure des Telecommunications, Paris, France, in 1965. He received the Doctorat Es-Sciences from the Faculty of Sciences of Paris in 1972.

From 1965 to 1967 he worked at Le College de France in high-energy physics. From 1967 to 1981 he worked at the Centre National d'Etudes des Telecommunications as an MTS, Group Leader, and Department Head. He joined Bell Laboratories, Holmdel, NJ, in 1981 and is presently the Head of the Quantum Physics and Electronic Research Department. He has been engaged in research on nonlinear optics of insulators, organic molecules and crystals, and semiconductors. He is currently interested in the optical response of microstructures under excitation by ultrashort and high-intensity light pulses.

Theodore C. Damen received the B.S.E.E. degree from the University of Eindhoven, Holland, The Netherlands, and the B.S. and M.S. degrees in physics from New York University, New York, in 1970 and 1972, respectively.

He joined Bell Laboratories, Holmdel, NJ, in 1958. With advent of the laser, his pioneering work provided the first experimental verification of group-theoretical predictions for light-matter interactions dealing with phonons, polaritions, plasmons, spin flip, surface modes and electron-hole

droplets, thereby contributing to the growth of a field which is still very much alive today. He was the first to observe laser action in a high density Neodymium Pentaphosphate crystal. He developed a semiconductor laser tunable over a very large bandwidth, and demonstrated an ultra fast modulator for CO_2 lasers. Currently, he has pioneered in the field of quantum confined Stark effect in quantum well structures.

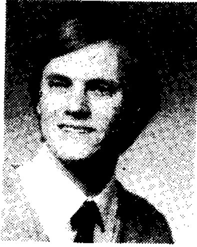

Thomas H. Wood (M'83) was born in Mineola, NY in 1953. He received the Sc.B. degree in physics from Brown University, Providence, RI. He received the M.S. and Ph.D. degrees in physics from the University of Illinois-Urbana, where he did work on light scattering from surfaces in ultrahigh vacuum. Since 1980 he has been at Bell Laboratories, and now works in their Crawford Hill, NJ, lab on optical quantum well devices and optical fiber systems.

Charles A. Burrus, Jr. (SM'63–F'74) was born in Shelby, NC, in 1927. He received the B.S. degree (cum laude) from Davidson College, Lexington, NC, in 1950, and the M.S. degree from Emory University, Atlanta, GA, in 1951, and the Ph.D. degree from Emory University in 1955, all in physics. At Duke University, Durham, NC, he studied under Texas Company and Shell Company fellowships, and was employed as a Research Associate from 1954 to 1955.

In 1955 he joined the Technical Staff of Bell Laboratories, Holmdel, NJ, where his work initially was concerned with the millimeter- and submillimeter-wave region of the spectrum (microwave spectroscopy and various types of semiconductor diodes for millimeter-wave use) and later with sources and detectors for lightwave communications (fiber-compatible LED's, lasers and p-i-n photodiodes). Currently he is engaged in work on both sources and detectors for lightwave communications in the 1–1.6 μm wavelength region, and on the effects of deuterium and hydrogen in optical fibers.

Dr. Burrus is a member of Phi Beta Kappa, Sigma Pi Sigma, and Sigma Xi. He is a Fellow of the American Association for the Advancement of Science, the American Physical Society, and the Optical Society of America. He was the recipient of the 1982 David Richardson Medal in applied optics from the Optical Society of America and the Distinguished Technical Staff Award (1982) from Bell Laboratories.

Arthur C. Gossard was born in Ottawa, IL, in 1935. He received the B.A. degree in physics from Harvard University, Cambridge, MA, in 1956 and the Ph.D. degree in physics from the University of California, Berkeley, in 1960.

He came to Bell Laboratories in 1960 and did research on nuclear and electron magnetic resonance in metals and magnetic materials. In 1974, he started work on molecular beam epitaxy, concentrating on the synthesis of very thin layers. He has published 180 papers and is presently a member of the Technical Staff in the Solid State Electronics Research Laboratory of AT&T Bell Laboratories, Murray Hill, NJ.

Dr. Gossard is a Fellow of the American Physical Society.

William Wiegmann was born in New York City in 1923.

He joined the Development Shops of Bell Laboratories in 1941 and shortly thereafter spent three years in the U.S. Air Force. After returning to Bell Laboratories he became involved in some of the early transistor and optoelectronic device development. For the past 13 years he has been involved in the MBE growth of GaAs and GaAlAs structures of all types as well as the engineering and fabrication of the MBE systems used in the growth process. He is presently a member of the Technical Staff in the Solid State Electronics Research Laboratory, Bell Laboratories, Murray Hill, NJ.